Article:
Huang, Jiahui, Fu, Weinong, Niu, Shuangxia et al. (2024) A Novel Dual-Side PM Machine with Decoupled Stator PM Topology. IEEE Transactions on Industrial Electronics. ISSN: 0278-0046

https://doi.org/10.1109/TIE.2024.3383009

A Novel Dual-Side PM Machine with Decoupled Stator PM Topology

Jiahui Huang, Weinong Fu, Shuangxia Niu, *Senior Member, IEEE*, Xing Zhao, *Member, IEEE*, and Yanding Bi

***Abstract*—Dual-side permanent magnet (DSPM) machines have gained attention with their high torque density and high efficiency. However, the topologies of the stator PM and stator core are constrained in the regular design, limiting the utilization of the stator PM. Consequently, the torque production of the stator side is limited. To overcome this constraint, this paper proposes a novel DSPM machine with a decoupled topology of stator PMs and iron core. The proposed design allows for optimal topologies of both components, enhancing the flux modulation effect in both the stator and rotor sides. This results in a generation of additional even-order harmonics of the equivalent stator magnetomotive force (MMF), thereby improving torque production on the stator side. Additionally, the placement of the stator split teeth can be evenly distributed along the stator bore, achieving an enhanced high-order harmonic of the stator permeance. Performance comparison between the conventional and proposed DSPM machines, following a global optimization, demonstrates that the proposed machine exhibits relatively high torque density and efficiency. Notably, the proposed machine achieves a 36.4% higher torque density while maintaining the same copper loss and PM usage. Finally, a prototype is manufactured and tested to validate the analysis.**

***Index Terms*—Dual-side PM machine, finite element analysis (FEA), flux modulation, torque density.**

I. Introduction

ORIGINATING from magnetic gears, flux modulation permanent magnet machines (FMPMMs) have emerged as a promising option for various applications, including electric vehicles, wind power generation, and direct-drive systems, owing to their inherent benefits of high torque density and efficiency[1]-[3]. Several types of flux modulation permanent magnet machines (FMPMMs) have been thoroughly studied [4],[5], such as Vernier machines [6], flux-switching permanent magnet machines (FSPMMs) [7], and flux reversal machines (FRMs) [8]. However, conventional FMPMMs have permanent magnets (PMs) placed only on either the stator or rotor. To further improve the torque density of these conventional single-side PM machines, dual-side PM (DSPM) machines have been proposed [9].

DSPM machines utilize permanent magnets on both the stator and rotor, enabling them to leverage the bi-directional flux modulation effect. To enable this effect, both sides should have flux modulators, which are presented by the teeth. The rotor PM magnetomotive force (MMF) is modulated by the stator teeth, while the stator PM MMF is correspondingly modulated by the rotor teeth. The rotors of DSPM machines commonly adopt a consequent-pole structure, with radially magnetized PMs or Halbach arrays embedded in the slots between rotor teeth [10]. The stator structures exhibit better diversification compared to the rotor structures, with open, semi-closed, or closed slot geometries options. Correspondingly, placement of the stator PMs affords comparable flexibility, as they can be located either in slot openings or at various tooth positions [11-15]. A DSPM machine with a Halbach array stator slot PM configuration has been proposed in [12], which achieves two times the back electromotive force (EMF) of the conventional machine, demonstrating simultaneous improvement in power factor and output torque. A group of spoke-type PMs sandwiched with iron poles is also placed in each stator slot opening to improve the torque density [13]. While open-slot DSPM machines with slot-opening PMs achieve superior torque density, the flux modulation poles are limited to the number of stator teeth. Hence, structures with PMs placed on stator tooth regions have been widely investigated to improve design flexibility. References [14] and [15] place stator PMs in split-tooth dummy slots, thoroughly exploring slot-pole combinations by using flux modulation theory. The structures with higher numbers of split-tooth are analyzed in [16] and [17]. Reference [18] proposes a structure that PMs alternatively mount on the stator teeth, with half the stator teeth enabling flux modulation. A comparison in [19] shows this structure achieves the highest torque density among four DSPM machine structures. To further enhance the torque density, structures with PMs inset on the tooth tips are evolved [20],[21]. Different PM arrangements of this kind of machine are comparative analyzed in [22], [23], and [24]. The results show that regardless of the number of PMs on each tooth, the structures with PMs placed in the same positions of each tooth exhibit optimal performance. Nonetheless, the aforementioned designs demonstrate a low PM utilization ratio on the stator side, which limits the torque density.

To address the issue of limited torque density, several topologies have been proposed. In addition to the existing

alternating surface-mounted PMs, tangentially magnetized magnets are placed within slot openings, achieving the flux-focusing effect of stator PMs [25]. Furthermore, spoke-type PMs embedded in stator teeth structures are proposed to increase torque density [26],[27]. To further enhance the flux-focusing effect and eliminate the flux barriers on the end portion of stator PMs, a DSPM machine with U-shaped stator PMs in teeth is proposed [28]. The proposed U-shaped DSPM machine effectively reduces the flux leakage.

In this paper, a novel DSPM machine with decoupled stator PMs from the stator core is proposed. The proposed DSPM machine adopts three sets of PMs, including spoke-type stator PMs, inset stator PMs, and inset rotor PMs. The spoke-type PMs, located in stator side dummy slots, do not occupy the entire slot, leaving space between the PMs and dummy teeth. This decouples spoke-type PMs from stator teeth, effectively reducing flux leakage and improving the stator PM utilization. The proposed structure and decoupling design principle are described in Section II. To investigate the multiple working harmonics to torque production, a hybrid finite element analysis (FEA)-analytical method combined with the frozen permeability method is adopted to reveal the working principle in Section III. Subsequently, to showcase the superiorities of the proposed design, the electromagnetic performance between the proposed DSPM machine and the conventional DSPM machine is compared in Section IV. A global optimization of both machines is conducted by using non-dominated sorting genetic algorithm II (NSGA-II) before comparison. To validate the performance prediction, a prototype is manufactured and tested in Section V. Finally, some conclusions are drawn in Section VI.

II. Machine Topology with Decoupled Structure

A. Machine Topology

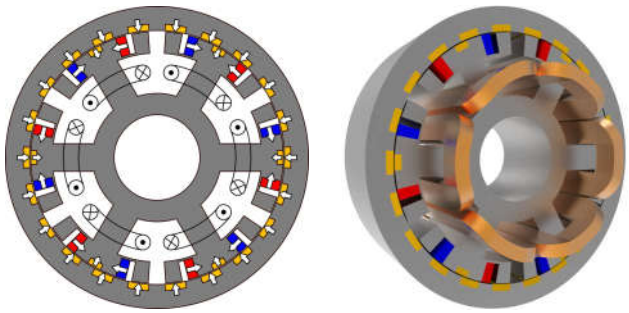

(a) (b)

Fig. 1. Topology of the proposed DSPM machine. (a) Front view. (b) Exploded view.

The proposed DSPM machine is shown in Fig. 1. It consists of a 6-slot single stator and a 22-pole pair single rotor with PMs on both parts. The rotor adopts the consequent-pole structure with PMs magnetized in the same radial direction and located between the rotor teeth. In addition to the rotor PMs, the stator part also includes two sets of PMs, namely a group of spoke-type PMs and inset stator PMs. The radial magnetized PMs are situated in the middle dummy slots in each stator tooth, while the spoke-type PMs are located in the side dummy slots. The groups of spoke-type PMs manifest a high flux concentrated effect. Furthermore, the spoke-type PMs, situated in stator side dummy slots, do not occupy the entire slot, hence leaving air between the PMs and dummy teeth. This serves to decouple spoke-type PMs from stator teeth, improving the stator PM utilization and enhancing the modulation effect of the rotor MMF. To reduce end length of armature winding and copper loss, a double-layer concentrated winding is used in the proposed machine. The main design parameters are listed in Table I.

TABLE I
Main Design Parameters of the Proposed Machine

Parameters	Values
Number of stator slots	6
Number of rotor pole pairs	22
Rotor outer diameter	150 mm
Stack length	50 mm
Air gap length	0.6 mm
Turns per phase	200
Rated speed	300 rpm
PM material	N35UH
Steel material	B35A360

B. Decoupling Design Principle for Optimal Structure

In conventional DSPM machines, the magnetic path of stator PMs are coupled with that of the stator teeth. This coupling introduces a constraint on the size of the stator PMs and teeth, which limits their ability to reach optimal values simultaneously. Specifically, when the size of the PMs is optimal, the modulation effect of the teeth is affected, which in turn affects the torque production of rotor PMs. Conversely, if the shape of the teeth is optimal, the utilization of the stator PMs cannot reach the optimal level. To overcome this limitation, a decoupling design concept is adopted in the stator structure. In the proposed design, the spoke-type PMs do not occupy the entire slot, allowing the stator PMs and stator teeth to both reach their optimal size and thus achieve the optimal torque production of both stator and rotor PMs.

On the one hand, the decoupled design allows the optimal design of the stator teeth, which is beneficial for the modulation of equivalent rotor MMF.

The permeance of the stator is given below.

$$\Lambda_s(\theta) = \Lambda_{s0} + \sum_{i=1}^{+\infty} \Lambda_{si} \cos(iN_s\theta) \tag{1}$$

where Λ_{s0} is the average value of the stator permeance, Λ_{si} presents the amplitude of the ith harmonic, N_s is the slot number, and θ is the angular position of the rotor.

The proposed machine has 22 rotor pole pairs and 6 main stator teeth with 4 split teeth on each of them. Due to the application of the decoupled structure, the stator teeth are able to distribute approximately evenly around the air gap, as shown in Fig. 2 (a). The FEA-predicted permeance waveform and its spectrum are shown in Fig. 2 (b) and (c), respectively. Both figures are presented using the per-unit system, and the amplitude of the 24 pole pairs harmonic is used as the base value. It can be found that the 24 pole pairs harmonic is very obvious. Additionally, 6, 12, 18, 30, and 48 pole pairs harmonics also exist to achieve the modulation effect involved in the torque generation. The rotor PMs excited MMF is mainly

modulated by the 24 pole pairs harmonic of stator permeance, which produces a 2 pole pairs working harmonic of air gap flux density that is coupled to the armature winding. It is one of the main working harmonics due to its high pole ratio that produces a significant portion of the output torque, which will be further investigated in the next section.

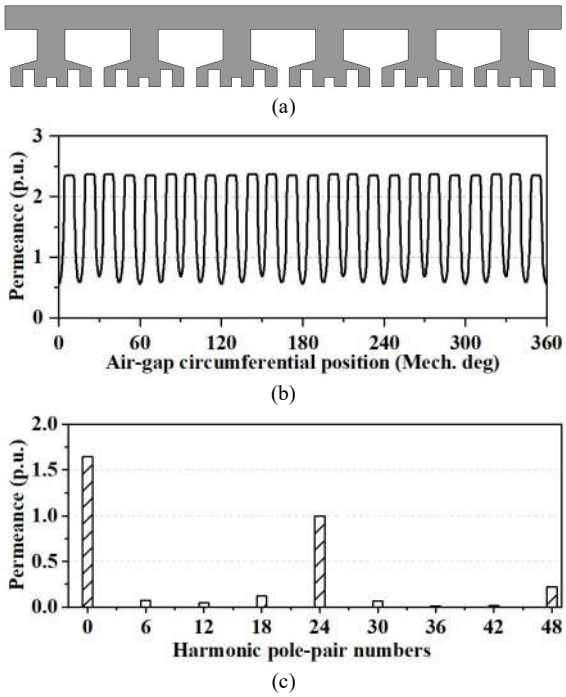

Fig. 2. Stator structure of the proposed machine and its permeance harmonics. (a) Detailed structure of the stator. (b) FEA-predicted permeance waveform of the stator. (c) Harmonics distribution.

On the other hand, the decoupling structure modifies the stator equivalent MMF waveform accordingly. The even-order harmonics are introduced in the proposed decoupled stator PM design. The simplified stator MMF waveforms of the regular design and the proposed design, which consider the excitation of stator spoke PMs and the permeance of the stator, are shown in Fig. 3 and Fig. 4, respectively. It can be observed in Fig.3 that the main harmonics in the conventional design correspond to the 6 pole pairs (n=1), 18 pole pairs (n=3), and 30 pole pairs (n=5) configurations, as indicated in (2). However, in the proposed design, not only odd-order harmonics (n=1,3,5...) exist, but even-order harmonics (n=2,4,6...) are also present, as shown in Fig. 4. Consequently, both odd and even-order harmonics contribute to torque production, achieving a notable improvement in torque density.

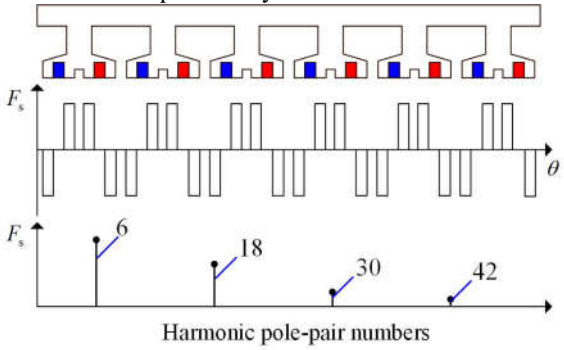

Fig. 3. Stator MMF of the machine with regular design.

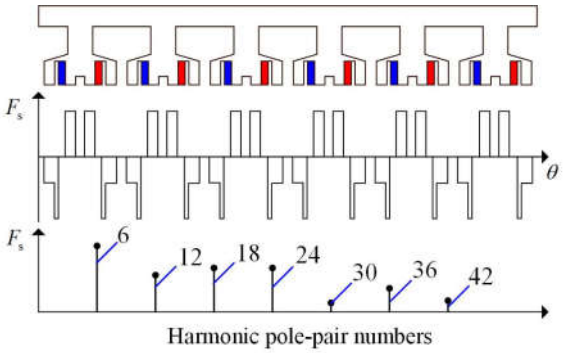

Fig. 4. Stator MMF of the machine with the proposed design.

The equivalent stator MMF with spoke-type PM excitation can be expressed as

$$F_{s\_spoke}(\theta)=\sum_{n}^{+\infty}F_{n\_spoke}\cos(nN_s\theta)$$
$$n=\begin{cases}1,3,5,7... & \text{regular design}\\ 1,2,3,4... & \text{proposed decoupled design}\end{cases} \quad (2)$$

where F_{n_spoke} denotes the magnitudes of stator MMF harmonics excited by spoke PM, and n is the order of the Fourier series. The 6 pole pairs harmonic is the fundamental harmonic (n=1).

III. Machine Working Principle

The DSPM machines can be regarded as a combination of the stator PM machines and the rotor PM machines. Consequently, the working principle of the DSPM machines can be simply explained by analyzing the effects of stator PMs and rotor PMs, respectively. To illustrate the working principle of the proposed machine, an MMF-permeance model is adopted.

The stator MMF, which considers the excitation of all stator PMs and the permeance of the stator, can be expressed as

$$F_s(\theta)=\sum_{n=1}^{+\infty}F_n\cos(nN_s\theta) \quad (3)$$

where F_n denotes the magnitudes of stator MMF harmonics.

The rotor permeance can be expressed as

$$\Lambda_r(\theta,t)=\Lambda_{r0}+\sum_{j=1}^{+\infty}\Lambda_{rj}\cos(jN_r(\theta-\Omega_r t)) \quad (4)$$

where Λ_{r0} is the average value of the rotor permeance, Λ_{rj} presents the amplitude of the jth harmonic, N_r is the rotor pole-pair numbers, j is the order of the Fourier series, Ω_r is the mechanical angular speed of the rotor.

Hence, the no-load air gap flux density produced by stator PMs can be derived as

$$\begin{aligned}B_{sg}(\theta,t)&=\frac{g}{\mu_0}F_s(\theta)\Lambda_r(\theta,t)\\&=\frac{g}{\mu_0}\Lambda_{r0}\sum_{n=1}^{\infty}F_n\cos(nN_s\theta)+\\&\quad\frac{g}{\mu_0}\sum_{n=1}^{\infty}\sum_{j=1}^{\infty}\frac{F_n\Lambda_{rj}}{2}\cos[(jN_r\pm nN_s)\theta-jN_r\Omega_r t]\end{aligned} \quad (5)$$

Similarly, rotor equivalent MMF, which considers the excitation of rotor PMs and the permeance of the rotor, can be expressed as

$$F_r(\theta,t)=\sum_{m=1}^{+\infty}F_m\cos[mN_r(\theta-\Omega_r t)] \tag{6}$$

where F_m denotes the magnitudes of rotor MMF harmonics, and m is the order of the Fourier series.

Consequently, the no-load air gap flux density excited by rotor PMs can be obtained as

$$\begin{aligned}B_{rg}(\theta,t)&=\frac{g}{\mu_0}F_r(\theta,t)\Lambda_s(\theta)\\&=\frac{g}{\mu_0}\Lambda_{s0}\sum_{m=1}^{\infty}F_m\cos[mN_r(\theta-\Omega_r t)]+\\&\frac{g}{\mu_0}\sum_{m=1}^{\infty}\sum_{i=1}^{\infty}\frac{F_m\Lambda_{si}}{2}\cos[(mN_r\pm iN_s)\theta-mN_r\Omega_r t]\end{aligned} \tag{7}$$

The synthetic no-load air gap flux density can be obtained as

$$B_g(\theta,t)=B_{sg}(\theta,t)+B_{rg}(\theta,t) \tag{8}$$

The winding function $N_a(\theta)$ can be expressed as

$$N_a(\theta)=\sum_{v=1}\frac{2}{v\pi}N_t k_{wv}\cos(v\theta) \tag{9}$$

Then, considering the flux interacting with phase A, the back electromotive force (EMF) of phase A can be obtained as

$$\begin{aligned}E_a(t)&=E_{sa}(t)+E_{ra}(t)\\&=-\frac{d}{dt}[r_g l_{st}\int_0^{2\pi}B_{sg}(\theta,t)N_a(\theta)d\theta]+\\&-\frac{d}{dt}[r_g l_{st}\int_0^{2\pi}B_{rg}(\theta,t)N_a(\theta)d\theta]\\&=\mathrm{sgn}(v)2r_g l_{st}N_t N_r\Omega_r\sin(N_r\Omega_r t)\sum_v^{\infty}\frac{B_{sgv}k_{wv}}{v}+\\&\mathrm{sgn}(v)\ 2r_g l_{st}N_t N_r\Omega_r\sin(N_r\Omega_r t)\sum_v^{\infty}\frac{B_{rgv}k_{wv}}{v}\end{aligned} \tag{10}$$

$$v=\left|N_r\pm iN_s\right|,\mathrm{sgn}(v)\begin{cases}1, & N_r\pm iN_s>0\\-1, & N_r\pm iN_s<0\end{cases} \tag{11}$$

where r_g is the air-gap radius, N_t is the number of turns per phase, v is the pole-pair number of space harmonics, and k_{wv} is the winding factor of vth harmonic. B_{sgv} and B_{rgv} are the vth air gap flux density excited by stator PMs and rotor PMs, respectively. Thus, the average torque can be given by

$$\begin{aligned}T_{avg}&=\frac{3}{2}\frac{E_a I_a}{\Omega_r}=\frac{3}{2}\frac{(E_{sa}+E_{ra})I_a}{\Omega_r}\\&=\mathrm{sgn}(v)3I_a r_g l_{st}N_t N_r\sum_v^{\infty}\frac{B_{sgv}k_{wv}}{v}+\\&\mathrm{sgn}(v)3I_a r_g l_{st}N_t N_r\sum_v^{\infty}\frac{B_{rgv}k_{wv}}{v}\end{aligned} \tag{12}$$

where I_a is the peak value of the phase current.

The frozen permeability (FP) method has been widely used to study issues related to magnetic saturation and cross-coupling, which can transform a non-linear issue into a linear one [29]. To accurately separate the torque contribution of stator PMs and rotor PMs, the FP method is utilized. Additionally, a combination of FEA and an analytical model is used to identify the contribution of harmonics to torque production. Fig. 5 illustrates the procedure for the entire process. The no-load non-linear FEA is firstly conducted with the excitation of both stator PMs and rotor PMs. Permeability distribution on the stator and rotor iron core is then frozen under this no-load condition. The linear FEA models with only stator PM excitation and rotor PM excitation are obtained based on the previous permeance distribution. Consequently, the no-load air gap flux densities for the stator PMs and rotor PMs can be obtained separately. Then, the no-load back EMFs and torque contributions of the main working harmonics can be quantified using (10) and (12).

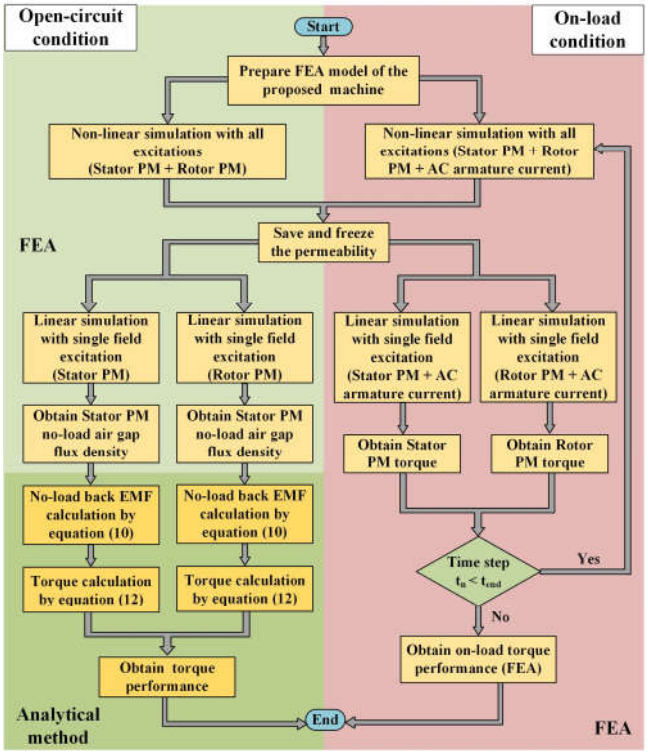

Fig. 5. Flow chat of the FEA-analytical method combined with FP method.

In parallel, the on-load non-linear FEA with the excitations of stator PMs, rotor PMs, and armature current is conducted. Permeability is frozen under this on-load condition. The torque produced by stator PMs and rotor PMs can be accurately separated. Finally, the average torque under certain steps can be obtained and compared to the value calculated by (12).

Fig. 6 (a) and (b) separately show the stator PM and rotor PM excited no-load air gap flux density waveforms with the utilization of the FP method. Their corresponding harmonic distributions are presented in Fig. 6(c) and (d). Obviously, the fundamental harmonic of the stator PM is 6 pole pairs, while that of the rotor PM is 22 pole pairs. It can be found that in the rotor PM part, the main working harmonics are the fundamental 22 pole pairs and the modulated 2 pole pairs harmonics. However, in the stator PM machine, the fundamental harmonic is stationary and cannot contribute to torque production. Consequently, except for the static harmonics (6, 18, 24,30…) that cannot contribute to torque production, the modulated 2

TABLE II
NO-LOAD BACK EMF AND TORQUE GENERATION OF MULTIPLE WORKING HARMONICS IN PROPOSED DSPM MACHINE

Working harmonics(v)	k_{wv}	sgn(v)	Stator PMs			Rotor PMs		
			B_{sg} (T)	E_{sg} (V)	T_{pms} (Nm)	B_{rg} (T)	E_{rg} (V)	T_{pmr} (Nm)
$N_r - 4N_s$, 2	-0.866	-1	0.0672	19.708	5.322	0.0914	26.806	7.239
$N_r - 3N_s$, 4	0.866	1	0.088	12.904	3.485	0.0158	2.317	0.626
$N_r - 5N_s$, 8	0.866	-1	0.0388	-2.845	-0.768	0.0464	-3.402	-0.919
$N_r - 2N_s$, 10	-0.866	1	0.0145	-0.85	-0.23	0.0104	-0.61	-0.165
$N_r - 6N_s$, 14	-0.866	-1	0.0151	0.633	0.171	0.0239	1.001	0.27
$N_r - N_s$, 16	0.866	1	0.1158	4.245	1.146	0.0395	1.448	0.391
$N_r - 7N_s$, 20	0.866	-1	0.003	-0.088	-0.024	0.0713	-2.091	-0.565
N_r, 22	0.866	1	/	/	/	0.7266	19.373	5.232
$N_r - 8N_s$, 26	-0.866	-1	0.0151	0.341	0.092	0.1132	2.554	0.69
$N_r + N_s$, 28	0.866	1	0.118	2.472	0.668	0.0223	0.467	0.126
$N_r - 9N_s$, 32	0.866	-1	0.0228	-0.418	-0.113	0.0247	-0.453	-0.122
$N_r + 2N_s$, 34	-0.866	1	0.0137	-0.236	-0.064	0.006	-0.104	-0.028
N_r - $10N_s$ 38	-0.866	-1	0.0328	0.506	0.137	0.016	0.247	0.067
Sum				36.372	9.822		47.553	12.842
Analytical result			Total Back EMF 83.923V			Total Torque 22.664Nm		
FEA result			Total Back EMF 85V			Total Torque 21.79Nm		

pole pairs and 4 pole pairs harmonics are the main working harmonics in the stator part.

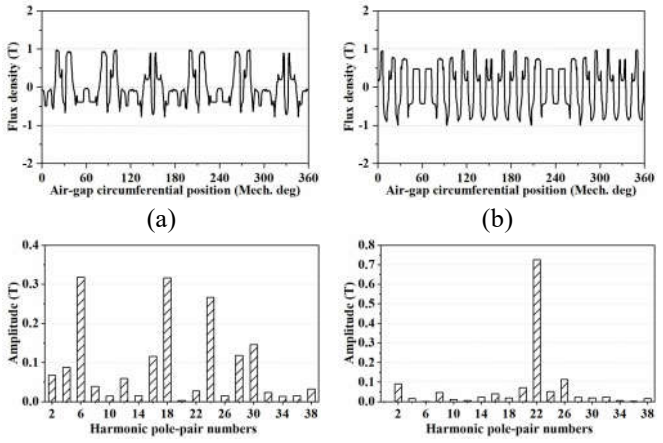

Fig. 6. Waveforms of no-load air gap flux densities and their harmonic distribution. (a) Stator PM excited waveform. (b) Rotor PM excited waveform. (c) Harmonic distribution of stator PM excited air gap flux density. (d) Harmonic distribution of rotor PM excited air gap flux density.

Using the amplitudes of air-gap flux density harmonics obtained from the FEA results, the no-load back EMF and torque performance can be determined through (10) and (12). Table II shows the contribution of the main working harmonics. It can be seen that 2 pole pairs and 4 pole pairs harmonics are the main working harmonics for the stator PM excitation. At the same time, 2 pole pairs and 22 pole pairs harmonics are the main working harmonics for the rotor PM excitation. The FEA results of the phase back EMF and output torque effectively confirm the analytical analysis.

IV. ELECTROMAGNETIC PERFORMANCE COMPARISON

To showcase the superiority of the proposed DSPM machine, the main electromagnetic performance of the proposed DSPM machine is quantitatively compared to a conventional DSPM machine, as shown in Fig. 7(a). The rotor of the conventional machine utilizes a consequent pole structure, which is similar to the proposed machine. Meanwhile, the stator incorporates a radially magnetized PM inserted into the dummy slot. To improve the conciseness, the conventional and proposed designs are referred to as Machine A and Machine B, respectively, in the following comparison part.

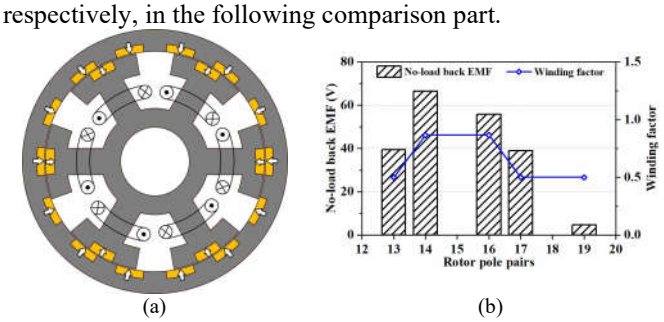

Fig. 7. Topology and selection of rotor pole pairs of the conventional machine. (a) Topology of the conventional machine. (b) Back EMF and winding factor under different rotor pole pairs.

A. Optimization

To ensure a fair comparison, both Machine A and Machine B are globally optimized for maximum output torque and minimum torque ripple. In addition, the pole-pair number of the conventional DSPM is selected as 14 to achieve the highest torque capability after investigating the influence of the pole-pair combinations of the conventional machine, as shown in Fig. 7(b). The optimization process for both machines is conducted under the same constraints, including overall size, stator slot numbers, air gap length, PM volume, and copper loss. The optimization results of both machines are presented in Fig. 8. The optimal designs of Machine A and Machine B, considering the tradeoff between torque and torque ripple, are identified and denoted by stars. The optimized design parameters of both machines are listed in Table III.

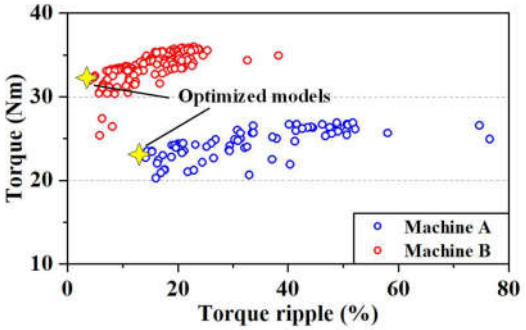

Fig. 8. Optimization results of Machine A and Machine B.

TABLE III
THE OPTIMIZED DESIGN PARAMETERS

Parameters	Machine A	Machine B
Outer diameter	150 mm	
Machine stack length	50 mm	
Air gap length	0.6 mm	
Copper loss	40 W	
PM volume	70 mL	
Rated speed	300 rpm	
Thickness of the outer rotor yoke	12 mm	8.7 mm
Thickness of rotor PM	3.5 mm	3.2 mm
Rotor PM pole arc coefficient	0.67	0.56
Thickness of spoke PMs in stator	/	9.64 mm
Width of spoke PM in stator	/	4.7deg
Thickness of stator mid PM	4.68 mm	3 mm
Width of stator mid PM	17.94 deg	6.5 deg
Height of stator tooth	18.9 mm	20 mm
Width of stator main tooth	13.2 mm	13.8 mm
Thickness of stator yoke	10 mm	10.6 mm

B. No-load Performance

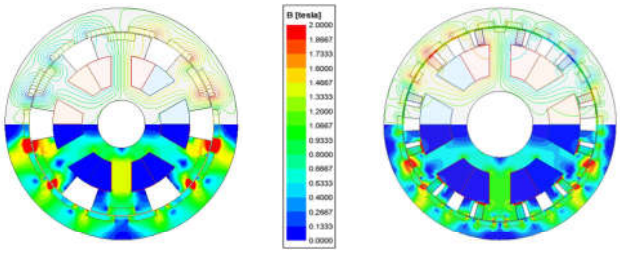

(a) (b)

Fig. 9. No-load flux distributions of both machines. (a) Machine A. (b) Machine B.

The no-load flux distributions of Machine A and Machine B are illustrated in Fig. 9. It can be observed that both machines experience a small portion of saturation in the stator and rotor tooth region. Machine A shows more severe saturation in the tooth region compared to Machine B. In addition, Machine B experiences saturation in the flux bridge region. Fig. 10 shows the waveforms and spectra of the no-load back EMF for both machines at the rotational speed of 300 rpm. It is evident that Machine B exhibits a 24.63% higher back EMF than Machine A. This increase signifies the superior torque performance of Machine B.

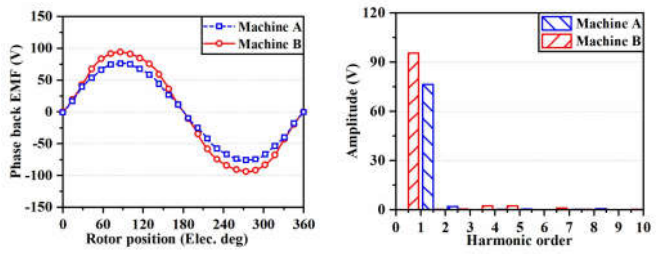

(a) (b)

Fig. 10. No-load back EMFs of both machines. (a) Waveforms. (b) Harmonics distribution.

C. On-load Performance

The rated torque waveforms of both machines, with the copper loss fixed at 40W, are presented in Fig. 11. Machine A achieves an average torque of 23.46 Nm, while the proposed Machine B achieves an average torque of 32 Nm, demonstrating a remarkable 36.4% increase in rated torque compared to Machine A. Furthermore, Machine B exhibits a much lower torque ripple compared to Machine A. Specifically, the torque ripples of Machine A and Machine B are 14.62% and 4.7%, respectively.

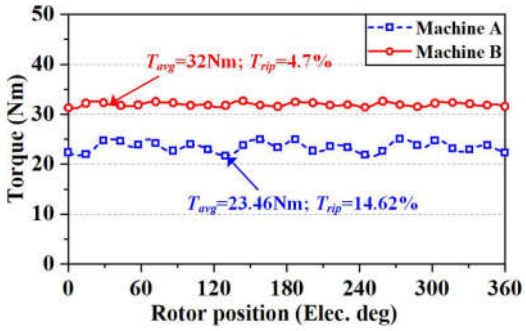

Fig. 11. Torque performance comparison.

Fig. 12 depicts the average torque versus input current curves for both machines. It can be observed that the average torques of Machine A and Machine B exhibit a nearly proportional increase when the current is below 7A. However, as the current exceeds this threshold, the increase in average torques for both machines begins to slow down. Nonetheless, the average torque of the proposed motor is notably higher than that of the conventional motor over the whole range of the current.

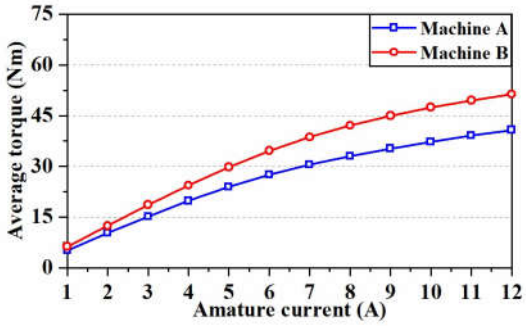

Fig. 12. Torque versus the input current curves.

D. Losses and Efficiency

Table IV presents a summary of the rated torque, torque ripple, losses, and efficiency characteristics of both machines under the rated condition. The copper losses of both machines are kept the same. Machine B has a higher core loss of 21.1W compared to Machine A, which has a core loss of 12.1W. This is mainly due to the lower pole-pair number of the Machine A, which is 14 compared to 22 in the Machine B. Nevertheless, Machine B maintains a higher efficiency than Machine A due to its larger output torque and power.

TABLE IV
ELECTROMAGNETIC PERFORMANCE COMPARISON

Items	Machine A	Machine B
Torque	23.46 Nm	32 Nm
Torque ripple	14.62%	4.7%
Copper loss	40 W	40 W
Core loss	12.1 W	21.1 W
PM eddy current loss	3.4 W	2.7 W
Efficiency	92.9%	94%

V. EXPERIMENTAL VALIDATION

A prototype of the proposed DSPM machine is fabricated and tested to validate the aforementioned FEA results. The

structural design parameters of the prototype align with the specifications presented in Table III, while the main components of the prototype are visually provided in Fig. 13. Specifically, Fig. 13(a) showcases the stator core and rotor core, whereas Fig. 13(b) illustrates the arrangement of tangentially magnetized PMs, radially magnetized PMs, and a concentrated armature winding within the stator. Additionally, Fig. 13(c) displays the rotor assembly, comprised of a rotor core and radially magnetized PMs.

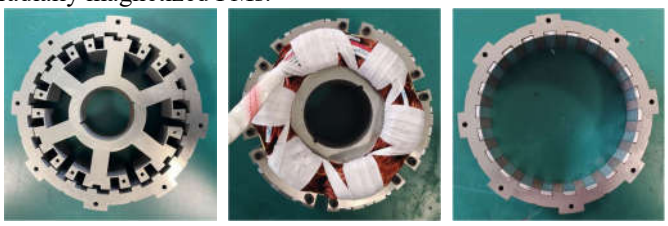

(a) (b) (c)

Fig. 13. Main components of the prototype. (a) Stator and rotor core. (b) Stator assembly. (c) Rotor assembly.

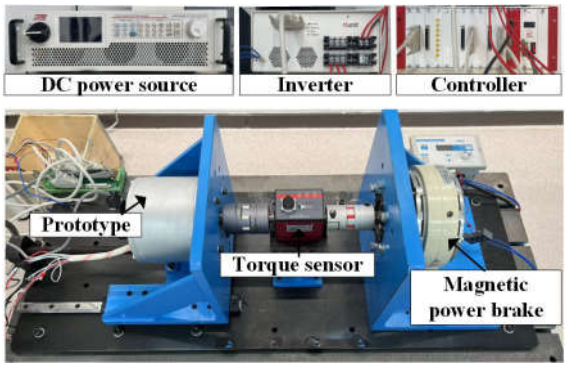

Fig. 14. The test rig of the proposed DSPM.

Fig. 14 shows the on-load test bench setup. The prototype is controlled by an inverter. The magnetic powder brake serves as a load, while the torque sensor is utilized to measure the dynamic torque. The prototype and magnetic powder brake are connected to the torque sensor via couplers.

Fig. 15 shows the FEA and measured phase back EMF waveforms of the proposed DSPM rotates at 300 rpm. The measured result is generally consistent with the FEA result, with a small deviation primarily attributed to end-effects and manufacturing tolerances. The measured torque-current angle curve at the rated current and the corresponding FEA result are presented in Fig. 16.

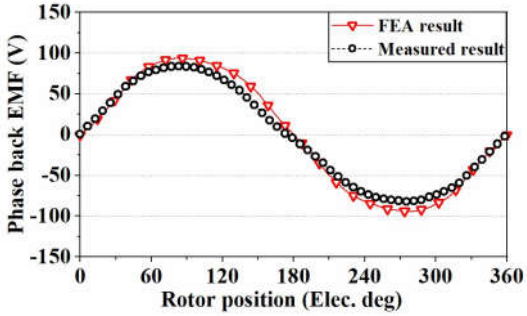

Fig. 15. Phase back EMF waveforms of the proposed DSPM machine.

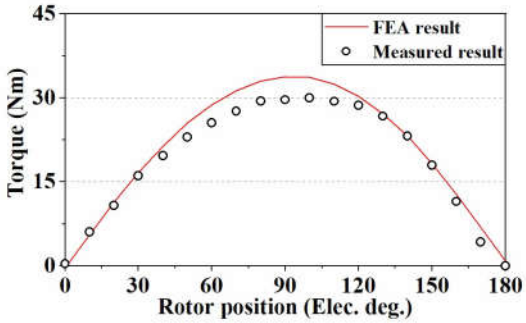

Fig. 16. Torque versus current angle curve of the proposed DSPM machine.

The torque waveforms of the measured and FEA results are shown in Fig. 17. The measured result is slightly lower than the FEA result. Furthermore, Fig. 18 displays the curves of average torque under different phase currents. It is observed that the growth rate of torque gradually decreases as the current increases. This phenomenon is due to the saturation effect of the iron core. Although there are slight discrepancies between the FEA and measured results, the experimental results generally align well with the FEA results. This serves to validate the effectiveness of the proposed DSPM machine design.

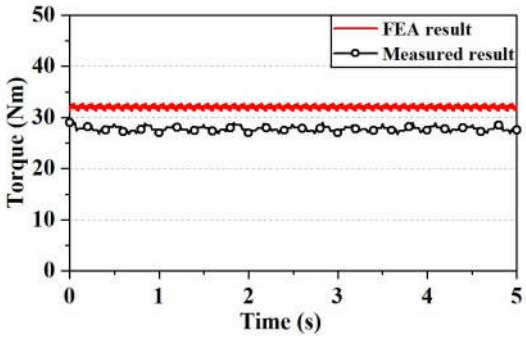

Fig. 17. Torque waveforms of the proposed DSPM machine.

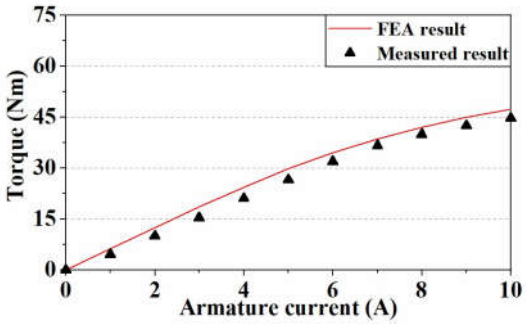

Fig. 18. Torque versus current curve of the proposed DSPM machine.

VI. Conclusion

This paper proposes a novel DSPM machine with a decoupled stator PM topology. The torque improvement mechanism of the proposed machine is revealed through the hybrid FEA & analytical method. By identifying and quantifying the working harmonics that contribute to torque production, it is found that the torque production mainly originates from two groups of air gap flux density harmonics.

The first category comprises harmonics with fewer pole pairs produced by the flux modulation effect. The second category consists of the fundamental harmonic of the rotor PMs. Compared to the conventional DSPM machine with the same PM volume and under the same copper loss, the proposed DSPM machine demonstrates a significant improvement in torque density of approximately 36.4%. Additionally, the proposed machine also exhibits improved efficiency. Finally, to validate the analysis, a prototype is manufactured and tested, and the experimental results confirm the analysis and simulation results.

ACKNOWLEDGMENT

This work was supported by the Research Grant Council, Hong Kong, China, under Project Polyu 152109/20E and Project C1052-21G.

REFERENCES

[1] S. Nategh et al., "A review on different aspects of traction motor design for railway applications," *IEEE Trans. on Ind. Applicat.*, vol. 56, no. 3, pp. 2148–2157, May 2020.

[2] Y. Chen, W. Fu, and X. Weng, "A concept of general flux-modulated electric machines based on a unified theory and its application to developing a novel doubly-fed dual-stator motor," *IEEE Trans. Ind. Electron.*, vol. 64, no. 12, pp. 9914–9923, Dec. 2017.

[3] Z. Z. Wu and Z. Q. Zhu, "Analysis of air-gap field modulation and magnetic gearing effects in switched flux permanent magnet machines," *IEEE Trans. Magn.*, vol. 51, no. 5, pp. 1–12, May 2015.

[4] X. Zhu, C. H. T. Lee, C. C. Chan, L. Xu, and W. Zhao, "Overview of flux-modulation machines based on flux-modulation principle: topology, theory, and development prospects," *IEEE Trans. Transp. Electrific.*, vol. 6, no. 2, pp. 612–624, Jun. 2020.

[5] M. Cheng, W. Hua, J. Zhang, and W. Zhao, "Overview of stator-permanent magnet brushless machines," *IEEE Trans. Ind. Electron.*, vol. 58, no. 11, pp. 5087–5101, Nov. 2011.

[6] B. Kim and T. A. Lipo, "Operation and design principles of a PM Vernier motor," *IEEE Trans. on Ind. Applicat.*, vol. 50, no. 6, pp. 3656–3663, Nov. 2014.

[7] Y. Bi, W. Fu, S. Niu, X. Zhao, J. Huang, and Z. Qiao, "Torque enhancement of a dual-PM flux-switching machine with improved multiple high-order working harmonics," *IEEE Trans. Transp. Electrific.*, pp. 1–1, 2023, doi: 10.1109/TTE.2023.3294189

[8] Y. Gao, D. Li, R. Qu, and J. Li, "Design procedure of flux reversal permanent magnet machines," *IEEE Trans. on Ind. Applicat.*, vol. 53, no. 5, pp. 4232–4241, Sep. 2017.

[9] A. Ishizaki, "Theory and optimum design of PM Vernier motor," in Seventh International Conference on Electrical Machines and Drives, Durham, UK: IEE, 1995, pp. 208–212. doi: 10.1049/cp:19950864.

[10] J. Huang, W. Fu, S. Niu, and X. Zhao, "Comparative analysis of different permanent magnet arrangements in a novel flux modulated electric machine," *IEEE Access*, vol. 9, pp. 14437–14445, 2021.

[11] L. Jian, Y. Shi, C. Liu, G. Xu, Y. Gong and C. C. Chan, "A novel dual-permanent-magnet-excited machine for low-speed large-torque applications," *IEEE Trans. Magn.*, vol. 49, no. 5, pp. 2381-2384, May 2013.

[12] K. Xie, D. Li, R. Qu, and Y. Gao, "A novel permanent magnet Vernier machine with halbach array magnets in stator slot opening," *IEEE Trans. Magn.*, vol. 53, no. 6, pp. 1–5, Jun. 2017.

[13] F. Wei, Z. Q. Zhu, H. Qu, L. Yan, and J. Qi, "New dual-PM spoke-type flux-reversal machines for direct-drive applications," *IEEE Trans. on Ind. Applicat.*, vol. 58, no. 5, pp. 6190–6202, Sep. 2022.

[14] Q. Lin, S. Niu, F. Cai, W. Fu, and L. Shang, "Design and optimization of a novel dual-PM machine for electric vehicle applications," *IEEE Trans. Veh. Technol.*, vol. 69, no. 12, pp. 14391–14400, Dec. 2020.

[15] L. Xu, W. Zhao, M. Wu, and J. Ji, "Investigation of slot–pole combination of dual-permanent-magnet-excited Vernier machines by using air-gap field modulation theory," *IEEE Trans. Transp. Electrific.*, vol. 5, no. 4, pp. 1360–1369, Dec. 2019.

[16] L. Xu, W. Zhao, G. Liu, J. Ji, and S. Niu, "A novel dual-permanent-magnet-excited machine with non-uniformly distributed permanent-magnets and flux modulation poles on the stator," *IEEE Trans. Veh. Technol.*, vol. 69, no. 7, pp. 7104–7115, Jul. 2020.

[17] D. K. Jang and J. H. Chang, "Design of a Vernier machine with PM on both sides of rotor and stator," *IEEE Trans. Magn.*, vol. 50, no. 2, pp. 877–880, Feb. 2014.

[18] Q. Wang, S. Niu, and X. Luo, "A novel hybrid dual-PM machine excited by AC with DC bias for electric vehicle propulsion," *IEEE Trans. Ind. Electron.*, vol. 64, no. 9, pp. 6908–6919, Sep. 2017.

[19] Q. Wang, S. Niu, and L. Yang, "Design optimization and comparative study of novel dual-PM excited machines," *IEEE Trans. Ind. Electron.*, vol. 64, no. 12, pp. 9924–9933, Dec. 2017.

[20] Y. Gao, M. Doppelbauer, J. Ou, and R. Qu, "Design of a double-side flux modulation permanent magnet machine for servo application," *IEEE J. Emerg. Sel. Topics Power Electron.*, vol. 10, no. 2, pp. 1671–1682, Apr. 2022.

[21] Y. Gao, M. Doppelbauer, R. Qu, D. Li, and H. Ding, "Synthesis of a flux modulation machine with permanent magnets on both stator and rotor," *IEEE Trans. on Ind. Applicat.*, vol. 57, no. 1, pp. 294–305, Jan. 2021.

[22] K. Yang, F. Zhao, and Y. Wang, "Analysis of Double-Layer Permanent-Magnet Flux Reversal Machines With Different Permanent Magnet Arrangements in Stator," *IEEE Trans. Magn.*, vol. 57, no. 2, pp. 1–5, Feb. 2021, doi: 10.1109/TMAG.2020.3005962.

[23] Y. Gao, T. Kosaka, Y. Liu, M. Doppelbauer, and R. Qu, "Comparative analysis of double flux modulation permanent magnet machines with different stator PM arrangements," *IEEE Trans. on Ind. Applicat.*, vol. 58, no. 2, pp. 1941–1951, Mar. 2022.

[24] Y. Zheng, W. Xiang, M. Kang, L. Wu, and Y. Fang, "Analysis of dual PM Vernier machines with different consequent-pole PM topologies," *IEEE Trans. on Ind. Applicat.*, vol. 59, no. 2, pp. 1670–1677, Mar. 2023.

[25] Y. Shi and L. Jian, "A novel dual-permanent-magnet-excited machine with flux strengthening effect for low-speed large-torque applications," *Energies*, vol. 11, no. 1, p. 153, Jan. 2018.

[26] Z. Liang, Y. Gao, D. Li, and R. Qu, "Design of a novel dual flux modulation machine with consequent-pole spoke-array permanent magnets in both stator and rotor," *Trans. Electr. Mach. Syst.*, vol. 2, no. 1, pp. 73–81, Mar. 2018.

[27] Y. Li, H. Yang, H. Lin, W. Liu, and S. Lyu, "A novel dual-sided PM machine with stator spoke-type PM structure," in 2019 IEEE Energy Conversion Congress and Exposition (ECCE), Baltimore, MD, USA: IEEE, Sep. 2019, pp. 1721–1728. doi: 10.1109/ECCE.2019.8912811.

[28] Y. Li, H. Yang, H. Lin, W. Liu, and X. Zhao, "Torque generation mechanism and performance evaluation of a dual-sided PM machine with stator U-shaped magnets," *IEEE Trans. on Ind. Applicat.*, vol. 58, no. 1, pp. 250–260, Jan. 2022.

[29] W. Q. Chu and Z. Q. Zhu, "Average torque separation in permanent magnet synchronous machines using frozen permeability," *IEEE Trans. Magn.*, vol. 49, no. 3, pp. 1202–1210, Mar. 2013.

Jiahui Huang received the B.Sc. degree in electrical engineering and automation from Xiamen University of Technology, China, in 2013, and the M.Sc. degree in electrical engineering from the Hong Kong Polytechnic University, Hong Kong, in 2015, where she is currently pursuing the Ph.D. degree in electrical engineering. Her main research interests include the design, analysis, and optimization of electric machines.

W. N. Fu obtained his Ph.D. from The Hong Kong Polytechnic University (PolyU) in 1999. He is a Professor at Shenzhen Institutes of Advanced Technology. He worked at PolyU about 13 years as an Associate Professor and Full Professor. He was one of the key developers at Ansoft Corporation in Pittsburgh, USA. He has about seven years of working experience at Ansoft, focusing on the development of commercial software Maxwell. Prof. Fu has made many contributions to the theory and application of electromagnetic field computation and electric device design, including the publication of over 250 refereed journal papers. Prof. Fu's research interests

mainly focus on computational electromagnetics, optimal design of electric devices, applied electromagnetics, and novel electric machines.

Shuangxia Niu (Senior Member, IEEE) received the B.Sc. and M.Sc. degrees from Tianjin University, Tianjin, China, and the Ph.D. degree from the University of Hong Kong, Hong Kong, SAR, China, all in electrical engineering. She is currently a professor with the Department of Electrical and Electronic Engineering, The Hong Kong Polytechnic University. She authored or coauthored more than 100 papers in leading journals. Prof. Niu is currently an Associate Editor for the IEEE Journal of Emerging and Selected Topics in Power Electronics.

Xing Zhao (Member, IEEE) received the B.Eng. degree from Nanjing University of Aeronautics and Astronautics, China, in 2014, and the Ph.D. degree from The Hong Kong Polytechnic University, Hong Kong SAR, in 2020, both in Electrical Engineering. Between Aug. 2020 and Oct. 2021, he served as a Research Assistant Professor with the Department of Electrical Engineering, The Hong Kong Polytechnic University. From Jul. 2019 to Jan. 2020, he was a Visiting Scholar with the Center for Advanced Power Systems, Florida State University, Tallahassee, USA. Currently, he is a Lecturer in the School of Physics, Engineering and Technology, University of York, UK. He has authored 75 technical papers in the international journals and conferences. His research interests include advanced electrical machines and power electronics for electric vehicles and renewable energy systems. He is an Associate Editor for IEEE Trans. Transportation Electrification, IEEE Trans. Energy Conversion, and IEEE Open Journal of the Industrial Electronics Society.

Yanding Bi received the B.Eng. degree in mechanical engineering from The Hong Kong Polytechnic University, Hong Kong, in 2019, where he is pursuing the Ph.D. degree in electrical engineering. His research interests include the design, analysis, and optimization of novel electric machines and magnetic gears for electric vehicles and renewable energy systems.